11370 *Biochemistry* **2009,** *48,* 11370–11380
DOI: 10.1021/bi901368e

BIOCHEMISTRY
including biophysical chemistry & molecular biology
Article

The 8 and 5 kDa Fragments of Plasma Gelsolin Form Amyloid Fibrils by a Nucleated Polymerization Mechanism, while the 68 kDa Fragment Is Not Amyloidogenic[†]

James P. Solomon,[‡] Isaac T. Yonemoto,[‡] Amber N. Murray,[‡] Joshua L. Price,[‡] Evan T. Powers,[‡] William E. Balch,[§] and Jeffery W. Kelly*[,‡]

[‡]*Departments of Chemistry and Molecular and Experimental Medicine and Skaggs Institute for Chemical Biology and* [§]*Departments of Cell Biology and Chemical Physiology and Institute for Childhood and Neglected Diseases, The Scripps Research Institute, 10550 North Torrey Pines Road, La Jolla, California 92037*

Received August 6, 2009; Revised Manuscript Received October 5, 2009

ABSTRACT: Familial amyloidosis of Finnish type (FAF), or gelsolin amyloidosis, is a systemic amyloid disease caused by a mutation (D187N/Y) in domain 2 of human plasma gelsolin, resulting in domain 2 misfolding within the secretory pathway. When D187N/Y gelsolin passes through the Golgi, furin endoproteolysis within domain 2 occurs as a consequence of the abnormal conformations that enable furin to bind and cleave, resulting in the secretion of a 68 kDa C-terminal fragment (amino acids 173−755, C68). The C68 fragment is cleaved upon secretion from the cell by membrane type 1 matrix metalloprotease (MT1-MMP), affording the 8 and 5 kDa fragments (amino acids 173−242 and 173−225, respectively) comprising the amyloid fibrils in FAF patients. Herein, we show that the 8 and 5 kDa gelsolin fragments form amyloid fibrils by a nucleated polymerization mechanism. In addition to demonstrating the expected concentration dependence of a nucleated polymerization reaction, the addition of preformed amyloid fibrils, or "seeds", was shown to bypass the requirement for the formation of a high-energy nucleus, accelerating 8 and 5 kDa D187N gelsolin amyloidogenesis. The C68 fragment can form small oligomers, but not amyloid fibrils, even when seeded with preformed 8 kDa fragment plasma gelsolin fibrils. Because the 68 kDa fragment of gelsolin does not form amyloid fibrils in vitro or in a recently published transgenic mouse model of FAF, we propose that administration of an MT1-MMP inhibitor could be an effective strategy for the treatment of FAF.

More than 30 human proteins can misassemble into cross-β-sheet aggregates, termed amyloid fibrils, by the multistep process of amyloidogenesis that appears to cause the degenerative diseases known as amyloid diseases (*1*−*4*). Some human amyloidogenic proteins are intrinsically disordered, whereas others adopt well-defined folded structures (*1*−*7*). Amyloidogenesis and aging together appear to lead to proteotoxicity, which is thought to cause the degeneration characteristic of the human amyloid diseases (*8*−*12*), clinically important examples of which include Alzheimer's disease, light chain amyloidosis, and the transthyretin amyloidoses (*8*, *13*−*17*). Amyloidogenesis by wild-type proteins or their fragments appears to cause sporadic amyloid diseases (*3*, *12*, *18*). In contrast, amyloidogenesis by mutant proteins or their fragments (which may or may not contain the mutation) appears to cause familial amyloidoses (*12*, *19*).

Gelsolin amyloid disease, also called familial amyloidosis of Finnish type (FAF),[1] appears to require a mutation in the plasma gelsolin protein (*20*−*23*) since there are no reports of wild-type plasma gelsolin aggregation leading to a sporadic amyloid disease. FAF is autosomal dominantly inherited, consistent with amyloidogenesis by a mutant plasma gelsolin fragment leading to a gain of toxic function (*19*, *20*). The mechanism of proteotoxicity, including whether intra- and/or extracellular amyloidogenesis lead to the degeneration characteristic of FAF, remains unclear (*19*). An aging-associated decline in cellular protein homeostasis capacity may contribute to the onset of the amyloidoses, including FAF, and may explain why aging is a dominant risk factor for these diseases (*8*, *10*−*12*, *19*).

FAF is characterized by systemic amyloid deposition, apparently facilitated by the extracellular matrix (*19*, *24*). Gelsolin fragment amyloid accumulation is particularly noticeable in the basement membrane of the skin (*25*), blood vessel walls (*26*), eyes (*27*), and the peripheral nervous system (*28*). Patients often present with corneal lattice dystrophy and a slowly progressive cranial and peripheral polyneuropathy. As the disease progresses, the skin becomes thickened and loose and the neuropathy is exacerbated, often with mild autonomic nervous system involvement (*26*). Ultimately, the amyloid deposition and the resulting inflammation in vital organs become life threatening, and thus, the primary causes of death are typically pneumonia, cerebral hemorrhage, or nephrotic syndrome (*28*, *29*).

[†]This research was supported by National Institutes of Health Grant AG018917, The Skaggs Institute for Chemical Biology, and the Lita Annenberg Hazen Foundation.

*To whom correspondence should be addressed. Phone: (858) 784-9601. Fax: (858) 784-9610. E-mail: jkelly@scripps.edu.

[1]Abbreviations: FAF, familial amyloidosis of Finnish type; C68, C-terminal 68 kDa fragment of human plasma gelsolin; MMP, matrix metalloprotease; MT1-MMP, membrane type 1 matrix metalloprotease; BCL-XL-1/2, B-cell lymphoma extra long (proteins fused to this domain are directed to inclusion bodies); EDTA, ethylenediamine-*N*,*N*,*N*′,*N*′-tetraacetic acid; Tris, tris(hydroxymethyl)aminomethane; MES, 2-(*N*-morpholino)ethanesulfonic acid; HPLC, high-pressure liquid chromatography; LC−MS, liquid chromatography−electrospray mass spectrometry; GST, glutathione *S*-transferase; TEV, tobacco etch virus; SDS−PAGE, sodium dodecyl sulfate−polyacrylamide gel electrophoresis; PG, full-length plasma gelsolin; Bis-Tris, 1,3-bis[tris(hydroxymethyl)methylamino]propane; ThT, thioflavin T; AFM, atomic force microscopy; AUC, analytical ultracentrifugation; ER, endoplasmic reticulum; βME, β-mercaptoethanol; DTT, dithiothreitol; TCEP, tris(2-carboxyethyl)-phosphine.

 Published on Web 11/11/2009

The amyloidogenic fragments that deposit in FAF patients derive from the protein gelsolin, a six-domain, Ca^{2+}-binding protein that regulates actin polymerization and fibril fragmentation (*30*, *31*). There are two splice variants of gelsolin: an 81 kDa intracellular variant responsible for remodeling the actin cytoskeleton and a secreted 83 kDa version that functions to scavenge actin fibrils released from injured tissue into the blood (thereby preventing increases in blood viscosity). Plasma gelsolin may also have other functions (*32*, *33*). Plasma gelsolin is secreted by several cell types, with muscle being a major source (*34*).

FAF is most often caused by a G654 to A point mutation in one gelsolin allele. This mutation changes an aspartate at position 187 to an asparagine (D187N), eliminating a calcium binding ligand and dramatically lowering the Ca^{2+} binding affinity of the second domain of plasma gelsolin, compromising its stability (*35*−*37*). A less common G654 to T point mutation, resulting in a tyrosine substitution at position 187 (D187Y), also causes FAF. Without Ca^{2+}-binding-mediated stabilization, domain 2 is conformationally heterogeneous, and the more extended conformers are susceptible to cleavage by furin in the trans Golgi, affording a C-terminal 68 kDa gelsolin fragment (C68), corresponding to amino acids 173−755 (*35*, *37*−*39*). Only a fraction of D187N/Y gelsolin is cleaved by aberrant furin endoproteolysis. The remainder is secreted as full-length plasma gelsolin that can adopt a folded tertiary structure similar to that of the wild type and appears to be adequately functional. Because D187N/Y homozygotes do not seem to exhibit a loss-of-function phenotype, and because gelsolin knockout mice are viable and exhibit only a mild, primarily hematological phenotype (*40*), the symptoms of FAF described above appear to derive from the gain of toxic function of mutant gelsolin. The C68 fragment is then cleaved by membrane type 1 matrix metalloprotease (MT1-MMP) or possibly other related MMPs in the extracellular matrix (*41*). The MMP(s) responsible likely derives from either the same cell as or cells adjacent to those secreting C68 (*19*). The MT1-MMP endoproteolysis of C68 results in the formation of 8 and 5 kDa amyloidogenic fragments, and the latter is not formed in the absence of the former. The 8 kDa fragment is the main component of FAF-associated fibrils (*19*, *42*).

The amyloidogenic 8 kDa plasma gelsolin fragment (amino acids 173−243 in the native full-length protein) incorporates the D187N mutation. This segment in the natively folded protein consists of four β-strands and an α-helix, but it is unlikely that the native structure is maintained in the fragment since endoproteolytic cleavage eliminates an internal β-strand (*43*). The 5 kDa amyloidogenic fragment (amino acids 173−225 in the native full-length protein), also incorporating the D187N mutation, is likely also intrinsically disordered as a monomer (*42*, *44*).

While the amyloidogenicity of the 8 kDa plasma gelsolin fragment has been previously studied (although not with rigorously monomerized peptides) (*24*, *45*), its amyloidogenicity relative to the other plasma gelsolin fragments has not been examined, nor has its mechanism of amyloid fibril formation been established. In addition, we wanted to know whether the secreted C68 fragment could form amyloid, as it is conceivable that the 8 and 5 kDa plasma gelsolin fragments composing human amyloid fibrils could result from C68 amyloidogenesis followed by further proteolytic digestion. Herein, we report that the 8 kDa fragment is more amyloidogenic than the 5 kDa fragment and that both the 8 and 5 kDa gelsolin fragments aggregate by a nucleated polymerization mechanism. We also demonstrate that C68 is not amyloidogenic, even upon attempted seeding by 8 kDa gelsolin fragment amyloid fibrils.

EXPERIMENTAL PROCEDURES

Production of 8 and 5 kDa Amyloidogenic Fragments in Escherichia coli. The 8 kDa fragment (amino acids 173−242) and the 5 kDa fragment (amino acids 173−225) of plasma gelsolin were biosynthesized as recombinant fusion proteins to BCL-XL-1/2, an aggregation-prone polypeptide that sequesters the attached gelsolin sequences into inclusion bodies within *E. coli* BL21(DE3), as previously described (*46*). Briefly, *E. coli* were grown to an OD_{600} of 1.2, induced with 5 mL of 20% arabinose, and grown for an additional 3 h. The bacteria were lysed by sonication in lysis buffer [50 mM Tris, 100 mM NaCl, 5 mM EDTA, and 0.02% NaN_3 (pH 8.0) with 0.1% Triton X added]. After centrifugation, the supernatant was removed, fresh lysis buffer was added to the pellet, and sonication was repeated to ensure complete lysis. After centrifugation, the remaining insoluble material, containing mostly inclusion bodies, was rinsed by sonication-facilitated resuspension followed by centrifugation once in 50 mM Tris, 100 mM NaCl, 5 mM EDTA, and 0.02% NaN_3 (pH 8.0) and then twice in 50 mM Tris, 50 mM MES, 100 mM NaCl, and 0.02% NaN_3 (pH 5.0). After the rinse steps, the inclusion bodies were dissolved in 7.2 M guanidine HCl for 5−7 days at 4 °C using rotary agitation. The protein was then purified using a Co column preequilibrated in 7.2 M guanidine HCl and 50 mM Tris (pH 8.0) utilizing the His_7 tag on the N-terminus of the BCL-XL-1/2 fusion protein. The protein was eluted in 7.2 M guanidine HCl, 50 mM Tris, and 50 mM MES (pH 5.0) through a reduction in pH. The fusion protein was then purified by reverse phase HPLC using a C-4 preparative column. When available, acetonitrile was used as the organic phase solvent, but a 50:50 mixture of 2-propanol and methanol was also used as an alternative organic phase solvent when acetonitrile was commercially unavailable. The fusion protein solution above was loaded onto the column equilibrated in water containing 0.2% trifluoroacetic acid and eluted with a linear gradient (from 20 to 80%) with a growing organic phase (containing 0.2% trifluoroacetic acid). The fusion protein was then lyophilized. At this stage, the BCL-XL-1/2 sequence was removed by cyanogen bromide cleavage. For the cleavage reaction, the lyophilized fusion protein was dissolved in 7.2 M guanidine HCl and 0.1 M HCl (pH < 1.0) at a concentration of 10 mg/mL, an equivalent volume of 5 mg/mL (roughly 100 molar equiv) CNBr in the same buffer was added, and the reaction proceeded overnight at room temperature. The crude cleavage product was purified by reverse phase HPLC using the solvent system described above, revealing $> 95\%$ purity. The 8 and 5 kDa plasma gelsolin fragments were characterized by LC−MS, and their masses matched the expected masses of 7860 and 6067 Da, respectively. A representative HPLC chromatogram and LC−MS characterization data from the purified 8 kDa fragment are shown in Figures 1 and 2 of the Supporting Information. The addition of the phosphine reducing agent, TCEP (4 mM), resulted in a 2 Da increase in mass, consistent with reduction of an intramolecular disulfide bond between cysteines at positions 188 and 201 that exists in the wild-type full-length gelsolin.

Monomerization of 8 and 5 kDa Gelsolin Fragments for Studies of Amyloidogenicity. The lyophilized 8 or 5 kDa gelsolin fragment (1−2 mg), purified as described above (the exact amount being dependent on the desired final concentration), was dissolved in 8 M guanidine HCl buffered with

50 mM sodium phosphate (pH 7.5) and sonicated in a water bath sonicator for 2 h to break up any aggregates or oligomers. The peptide solution was then loaded onto a Superdex 30 gel filtration column (20 mL volume) preequilibrated with 50 mM sodium phosphate and 100 mM NaCl (the pH of the buffers was between 6.0 and 7.5, depending on the experiment) to buffer exchange and remove any aggregated species. Oligomers eluted from the column in the void volume at ~8 mL, while the monomerized peptides eluted at 12 mL. The monomerized peptide in the desired buffer, free of chaotrope, was collected and used immediately in the amyloidogenicity experiments.

Production of the 68 kDa C-Terminal Fragment (C68) in E. coli. Recombinant C68 was made as an N-terminal glutathione *S*-transferase (GST) fusion protein featuring a His_6 tag N-terminal to the GST sequence (His_6−GST−TEV cleavage site−C68), as previously described (*45*), with minor modifications. The TEV protease cleavage site was added for the specific and efficient removal of the solubilization protein and purification tag from the 68 kDa fragment of interest, and the fusion protein was purified using a Ni column, as it was determined that the fusion protein did not bind well to the glutathione resin. Bacterial lysate was loaded onto the Ni column preequilibrated in 20 mM Tris and 10 mM imidazole and was eluted using a linear gradient to 250 mM imidazole over three column volumes. The fractions containing the fusion protein were collected and pooled. TEV protease was added in a 1:100 molar ratio to cleave His_6−GST from C68, and glycerol was added to a final concentration of 20% to prevent protein aggregation. The cleavage reaction solution was mixed and then incubated overnight, without stirring, at 4 °C. A reverse Ni column strategy was then utilized to purify C68 from the other cleavage products and the TEV protease (which also has a His_6 tag). Ni resin was added directly to the cleavage reaction mixture and incubated for 2 h at 4 °C. With the addition of the glycerol and the Ni resin, the imidazole concentration was substantially diluted, allowing the His_6−GST purification tag and the TEV protease to bind efficiently to the Ni resin. The flow-through, containing the purified C68, was then collected and concentrated using a centrifugal protein concentrator. Because C68 is a large, multidomain protein with folded domains, it was not pretreated with guanidine, as the 8 and 5 kDa fragments were, for the purpose of monomerization. However, it was still subjected to a final purification and monomerization step by being passed through a Superdex 200 gel filtration column (20 mL volume column) that had been preequilibrated with 50 mM sodium phosphate and 100 mM NaCl (pH of the buffers was between 6.5 and 7.5, depending on the experiment) to buffer exchange and remove any aggregated species immediately before any experiments were performed. SDS−PAGE revealed >95% purity (Figure 3 of the Supporting Information).

Production of Full-Length Plasma Gelsolin (PG). The pET3a construct for PG (obtained as a kind gift from the laboratory of H. L. Yin, University of Texas Southwestern Medical Center, Dallas, TX) enabled expression in *E. coli* BL21(DE3) cells and gelsolin was purified by a method based on the one reported by the Yin laboratory (*47*). Briefly, *E. coli* cells transfected with the construct were grown at 37 °C to an OD_{600} of 0.6, induced by addition of 1 mM isopropyl 1-thio-β-D-galactopyranoside, and allowed to grow for an additional 3 h. Cells were lysed by sonication in multiple 5 s bursts on ice, aided by the addition of 1 mg of lysozyme. The lysate was centrifuged for 10 min at 10,000*g* at 4 °C. Because SDS−PAGE revealed most of the PG to be in the supernatant, the supernatant was filtered with a 0.45 μm filter and loaded onto a Source Q anion exchange column preequilibrated with 20 mM Bis-Tris and 0.02% NaN_3 (pH 7.0). The bound PG was eluted with a gradient of NaCl (from 0 to 0.5 M). Because PG is a large, multidomain protein with folded domains, it was not pretreated with guanidine. Instead, it was passed through a Superdex 200 gel filtration column (20 mL volume column) that had been preequilibrated with 50 mM sodium phosphate and 100 mM NaCl (pH of the buffer was between 6.5 and 7.5, depending on the experiment) to buffer exchange and remove any aggregated species immediately before any experiments were performed. SDS−PAGE revealed >90% purity (Figure 4 of the Supporting Information).

Preparation of Fibril Seeds for Seeding Experiments. Monomerized 8 or 5 kDa gelsolin fragments (20 μM) were aggregated in 50 mM sodium phosphate, 100 mM NaCl, and 0.02% NaN_3 (pH 7.0) at 37 °C in an microfuge tube (wherein the final volume was at least 600 μL) under constant agitation using an overhead shaker (24 rpm) for at least 16 h. It was critical that the final volume was at least 600 μL; otherwise, the surface tension does not allow the solution to mix with each rotation. The presence of fibrils was verified by thioflavin T(TfT) fluorescence. The fluorescence signal should be at least 10 times that of a solution of 20 μM TfT with no protein. Preformed fibrils were used in experiments within 3 days, after which the magnitude of the TfT signal decreased dramatically. Immediately before use in the seeding experiments, the gelsolin fibrils were sonicated for 20 min in a water bath sonicator, as this has been previously shown with amyloid β to disrupt long fibrils into more uniform 50−100 nm fibrils (previously characterized by AFM) more suitable for a seeding experiment (*8*, *48*).

Thioflavin T Aggregation Assay Utilizing a Plate Reader. The monomerized amyloidogenic gelsolin fragments were diluted to the desired concentration in 50 mM sodium phosphate buffer with 100 mM NaCl, 0.02% NaN_3, and 20 μM TfT (pH of the buffer was between 6.0 and 7.5, as reported in Results). For assessing the amenability to seeding, a fraction of the amyloidogenic gelsolin fragment concentration (ranging from 0.1 to 10%, as reported in Results) was added as preformed fibril seeds, prepared as described above, instead of monomerized peptide. For experiments involving extracellular matrix components, the oligosaccharides were dissolved in buffer and added to the solution to achieve the reported concentration. All components were mixed together in an Eppendorf tube, and 97 μL of each solution was transferred to a well of a 96-well microplate in triplicate (black plate with clear bottom, Corning Inc., Corning, NY). The plate was sealed with an airtight lid to minimize evaporation and then placed in a Gemini SpectraMax EM fluorescence plate reader (Molecular Devices, Sunnyvale, CA) and incubated at 37 °C for the duration of the experiment. Every 10 min, the fluorescence (excitation at 440 nm and emission at 485 nm) was measured from the bottom of the plate after it had been shaken for 5 s. Each reading was the mean of 30 individual scans. The data from the triplicate wells were averaged and plotted as TfT fluorescence versus time.

Thioflavin T Fluorescence Amyloidogenicity Assay Utilizing a Fluorescence Spectrometer. To confirm the validity of the data obtained from the plate reader, additional experiments were performed using a fluorescence spectrometer. The monomerized solution of the gelsolin fragment was diluted to the desired concentration in 50 mM sodium phosphate buffer with 100 mM NaCl and 0.02% NaN_3 (pH of the buffers was between

6.5 and 7.5, as reported in Results). For experiments involving extracellular matrix components, the oligosaccharides were dissolved in the same buffer and added to the solution. All components were mixed together in an Eppendorf tube in which the final volume was at least 600 μL. The tubes were placed in a 37 °C incubator and mixed using overhead rotation at 24 rpm. Periodically, 15 μL of the solution was removed, added to 85 μL of a 23.5 μM TfT solution (final TfT concentration of 20 μM), and transferred to a fluorescence cuvette. The fluorescence (excitation at 440 nm and emission at 485 nm) was then measured in a Cary Eclipse fluorescence spectrophotometer, and the data were plotted as fluorescence versus time. Aliquots could also be taken from these samples for examination by other techniques, as described below.

Atomic Force Microscopy (*AFM*). Aliquots from samples prepared for the fluorimeter-based thioflavin T aggregation assay described directly above were examined by AFM to discern aggregate morphology. Twenty microliters of the sample was adsorbed to a surface of freshly cleaved mica for 1 min. The liquid was then wicked off the surface of the mica with filter paper. Salt and unbound material were removed when the sample was washed three times with 25 μL of distilled water that was immediately wicked off of the surface of the mica with filter paper. AFM images were recorded in tapping mode using a Digital Instruments multimode scanning probe microscope with a Nanoscope IIIa controller and force modulation etched silicon probes.

Analytical Ultracentrifugation (*AUC*). Samples prepared for the fluorimeter-based thioflavin T aggregation assay described above were examined by AUC. Sedimentation velocity experiments were performed on a Beckman XL-I analytical ultracentrifuge using both absorbance and interference optics. Protein samples were loaded into 1.2 cm cells and were allowed to equilibrate for 1 h at 25 °C prior to centrifugation at 50,000 rpm in an An60-TI four-hole rotor. Data were analyzed using the $c(s)$ method in Sedfit (*49*).

Proteinase K-Limited Digestion. Monomerized 8 or 5 kDa gelsolin (20 μM) was subjected to overhead rotation (24 rpm) at 37 °C for 16 h at pH 7.0 to form fibrils, as in the fluorimeter-based thioflavin T aggregation assay described above. The presence of fibrils was verified by TfT fluorescence. Proteinase K (3 μL of a 0.1 mg/mL solution) was added to 100 μL of the fibril solution and incubated at 37 °C with continuous orbital shaking (250 rpm) for various lengths of time before inactivation of the proteinase K by boiling for 10 min.

For SDS−PAGE analysis, gel loading buffer was added to the proteinase K-treated fibrils, and the samples were boiled for 10 min. Samples were run on a 16.5% Tris/Tricine peptide gel to separate the small peptide fragments (*50*), and the gel was stained with Coomassie blue for analysis. For mass spectrometry analysis, 90 μL of 8 M guanidine HCl (pH 4.0) was added to 10 μL of the digested fibrils and that sample was incubated for 6 h before being examined by LC−MS.

RESULTS

The Relative Amyloidogenicity of the 68, 8, and 5 kDa Plasma Gelsolin Fragments. The aggregation propensity of the monomerized gelsolin fragments was examined as a function of pH using the plate reader TfT fluorescence amyloidogenicity assay, as described in Experimental Procedures. It was previously shown that aggregation of the 8 kDa plasma gelsolin fragment is very sensitive to pH: amyloidogenicity is enhanced as the pH decreases, consistent with the calculated pI (5.36) of this fragment (*45*). However, in the prior study, a rigorous monomerization pretreatment was not performed; hence, it is important to collect revised data to ensure that fibrillar seeds were not contributing to the previous observations. Decreasing the pH should lower the net charge on this intrinsically disordered fragment, rendering it more assembly competent at a given concentration (*51*). Figure 1A illustrates the pH dependence of the amyloidogenicity of the 8 kDa fragment. Reducing the pH dramatically accelerates formation of 8 kDa plasma gelsolin amyloid fibrils.

Because the aggregation kinetics exhibited by the 8 kDa fragment of plasma gelsolin are highly pH dependent, a comparison of the relative amyloidogenicities of the C68, 8 kDa, and 5 kDa gelsolin fragments was performed at several physiologically relevant pHs (6.5−7.5). The physiological concentration of gelsolin in human plasma averages 200 μg/mL in healthy volunteers (2.5 μM), with higher levels often seen (*34*). We therefore decided to examine the amyloidogenicity of the fragments at a concentration of 4 μM, as this concentration is in the physiologically relevant range, is sufficiently high to facilitate aggregation on a convenient laboratory time scale, and allows for an excellent signal-to-noise ratio in the TfT-monitored amyloidogenicity time courses.

At the lowest pH examined (pH 6.5), the 8 and 5 kDa gelsolin fragments exhibited nearly identical amyloidogenicity rates, while the C68 fragment exhibited only a slight increase in the level of TfT binding (Figure 1B). Both the 8 and 5 kDa fragments exhibit time courses expected of a nucleated polymerization, featuring a lag or nucleation phase (~2 h), a growth phase with a t_{50} of 6.5 h, and a stationary phase, reached when the monomer is depleted below the critical concentration. The C68 curve does not show these characteristic phases.

At pH 6.8, the 8 kDa fragment again exhibited an amyloidogenicity time course consistent with a nucleated polymerization, although aggregation was slower (Figure 1C). In contrast, the 5 kDa fragment did not aggregate at pH 6.8, implying that at this pH the concentration of the 5 kDa fragment is now below its critical concentration, that the time frame of the experiment was too short for observation of any aggregation and increase in the magnitude of the TfT signal, or that the 5 kDa fragment simply does not aggregate at pH 6.8. The C68 fragment exhibited an increase in TfT fluorescence with time, and although it reached the amplitude of that of the 8 kDa fragment, it did not exhibit a lag phase followed by a growth phase. Two explanations for the increase in TfT fluorescence are that C68 is forming reversible oligomers or that it is aggregating into fibrils by a downhill polymerization like transthyretin does (*52*). It is well established that TfT is an environment-sensitive fluorophore that reliably reports on amyloid fibril formation (*53*), but there are also examples of TfT exhibiting fluorescence when bound to a native or near-native protein (*54*). These possibilities will be examined below. Full-length recombinant plasma gelsolin (PG) was also examined at pH 6.8, revealing that TfT fluorescence did not increase with time. It is notable that the amplitudes of the TfT fluorescence at time zero from both C68 and PG are nearly identical and substantially greater than that of the buffer control or those of the monomeric 8 and 5 kDa fragments at the beginning of their aggregation reactions, indicating that there are one or more TfT binding sites in PG and C68, likely in a folded domain(s) common to both.

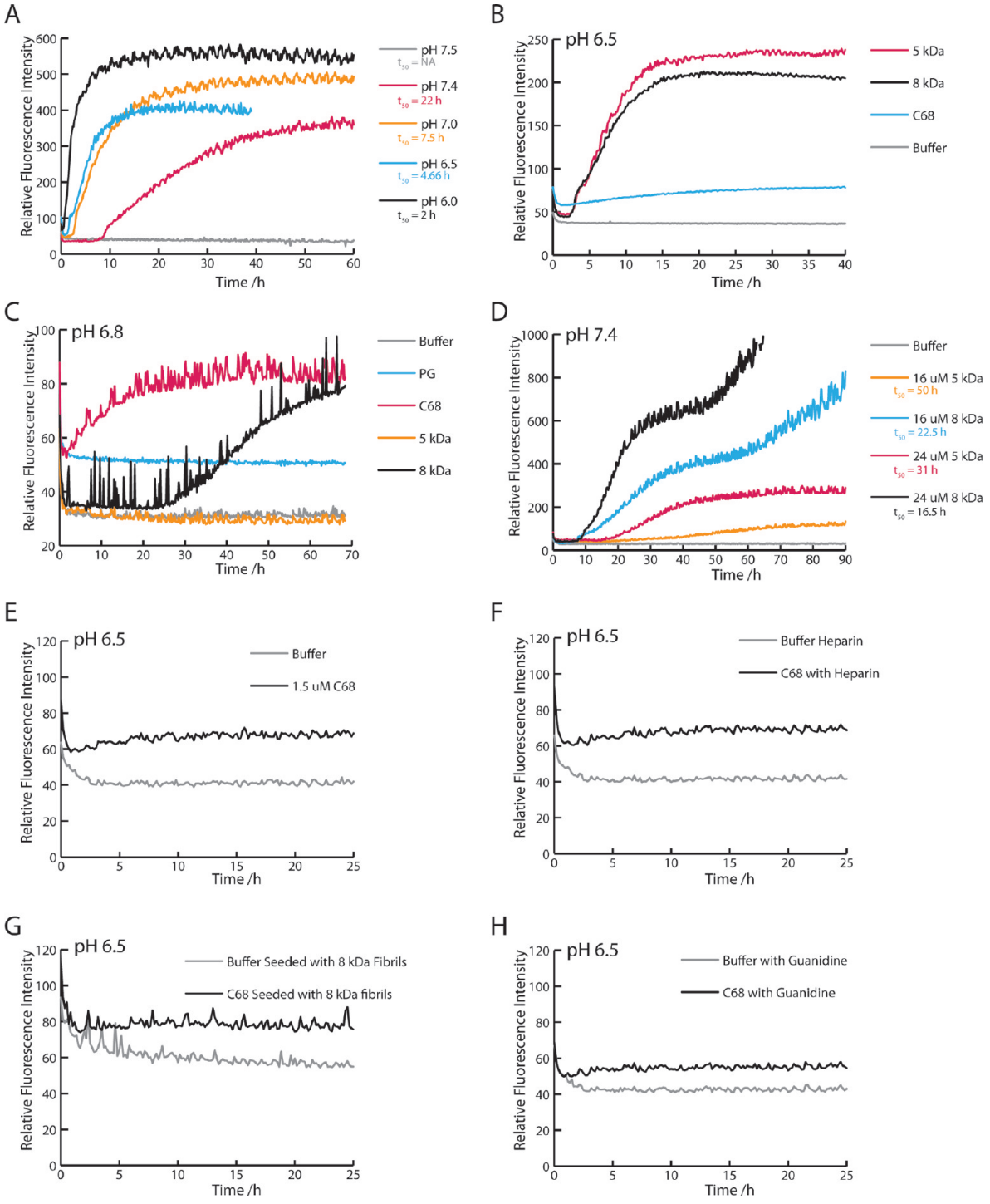

FIGURE 1: Relative amyloidogenicity of the 68, 8, and 5 kDa plasma gelsolin fragments (corresponding to amino acids 173−755, 173−242, and 173−225, respectively). Aggregation was monitored by the increase in TfT fluorescence in the plate reader TfT aggregation assay (see Experimental Procedures for details). The t_{50} associated with each curve is defined as the time required to reach half the maximum fluorescence and is shown in the legends of panels A and D. (A) The freshly monomerized 8 kDa fragment (8 μM) was assayed at pHs varying from 6.0 to 7.5. (B and C) Plasma gelsolin and fragments thereof (4 μM) were examined by the TfT fluorescence plate reader assay at pH 6.5 (B) and 6.8 (C). (D) Comparison of the amyloidogenicity of the 8 and 5 kDa fragments at higher concentrations (pH 7.4). (E−H) Various conditions known to promote amyloid fibril formation were applied to C68 (1.5 μM) at pH 6.5. (E) Buffer alone, control series as a reference for panels F−H. (F) Heparin (10 μg/mL) was added to the C68 solution. (G) Preformed 8 kDa fibrils were sonicated to generate fibrils of uniform length which were then added to the C68 solution. (H) Guanidine HCl (0.5 M) was added to the C68 solution.

The 68, 8, and 5 kDa gelsolin amyloidogenicity experiments were also conducted at pH 7.0 and 7.4. The 5 kDa fragment was not amyloidogenic on this time scale, in contrast to the 8 kDa fragment, which exhibited a slight increase in TfT fluorescence, consistent with inefficient fibril formation at these pHs (Figure 5 of the Supporting Information). The C68 fragment exhibited a similar TfT fluorescence increase with time as observed at the lower pHs, as discussed above (Figure 5 of the Supporting Information).

The amyloidogenicity of the 8 and 5 kDa fragments was further examined at pH 7.4 as a function of gelsolin fragment concentration (Figure 1D). The 8 kDa fragment formed amyloid

much more quickly than the 5 kDa fragment at these higher concentrations. With the exception of the data collected at pH 6.5, the 8 kDa fragment is more amyloidogenic than the 5 kDa fragment under all other conditions explored (physiological concentrations and pH).

It is important to note that the first few points of the TfT plate reader amyloidogenicity time-courses have a higher fluorescence reading than the baseline. It was determined that this is an artifact of the instrument and does not represent binding of TfT to β-sheet structures, as buffer with TfT added also exhibits the higher initial reading (Figure 1). Because the initial reading is always ~20 raw fluorescence units higher than the baseline, the artifact is more pronounced when the curve has a smaller maximum fluorescence, as in the experiments with gelsolin fragments at a concentration of ≤ 4 μM (e.g., Figure 1B,E,F).

To further probe the apparent aggregation of the C68 fragment, we examined its aggregation under conditions known to accelerate amyloidogenesis (Figures 1E−H). All experiments were performed using 1.5 μM C68 at pH 6.5. First, heparin (10 μg/mL) was added to the reaction mixture, as heparin has been shown to accelerate formation of 8 kDa gelsolin fragment amyloid fibrils (*24*). When compared to the control (Figure 1E), no acceleration or amplitude increase in the TfT time course was observed (Figure 1F). Nearly all amyloidogenicity reactions are accelerated by sulfonated or sulfated glycosaminoglycan polymers (*55*, *56*), making it unlikely that C68 is forming amyloid. Second, sonicated 8 kDa fibrils were added to monomerized C68 in an attempt to nucleate amyloid fibril formation. TfT did bind to the 8 kDa fibril seeds, which can be seen by the increase in the TfT fluorescence baseline relative to the other experiments, but these seeds clearly did not template the fibrillization of C68 (Figure 1G), providing further evidence that it is unlikely that the C68-mediated increase in the magnitude of the TfT signal with time is a consequence of amyloid fibril formation. Finally, 0.5 M guanidine was added to C68, because chaotropes are known to destabilize initially folded amyloidogenic proteins, or collapsed intrinsically disordered proteins, accelerating the process of fibril formation (*57*). However, no increase in the magnitude of the TfT signal, linked to amyloidogenicity, was observed (Figure 1H).

Next, we attempted to maximize the probability for C68 amyloid fibril formation by using a different agitation method, as the method of agitation can be an important factor in inducing amyloidogenesis (*58*). The C68 fragment (4 μM) was subjected to constant rotation at 37 °C (24 rpm) both in the presence and in the absence of heparin (10 μg/mL), at pH 6.5, utilizing the fluorimeter-based TfT assay described in Experimental Procedures. Constant rotation maximizes the chance for aggregation because of the constant exposure of C68 to the denaturing air−water interface (*59*−*61*). A slight increase in TfT fluorescence was observed, comparable to that derived from the plate reader assays described above, but no evidence for amyloidogenesis of C68 was noted (Figure 6A of the Supporting Information).

To determine whether this small increase in the magnitude of the C68 TfT signal with time was due to the oligomerization of C68 and TfT binding, the solution was examined by AFM and analytical ultracentrifugation (AUC) at the conclusion of the fluorimeter-based TfT assay. AFM did not detect the presence of any large oligomers or amyloid fibrils, as the surface of the mica looks very similar to the buffer control (Figure 6 of the Supporting Information, cf. panel B to panel C). In contrast, when a solution of the 8 kDa gelsolin fragment (4 μM) is subjected to constant rotation at 37 °C (24 rpm) overnight,

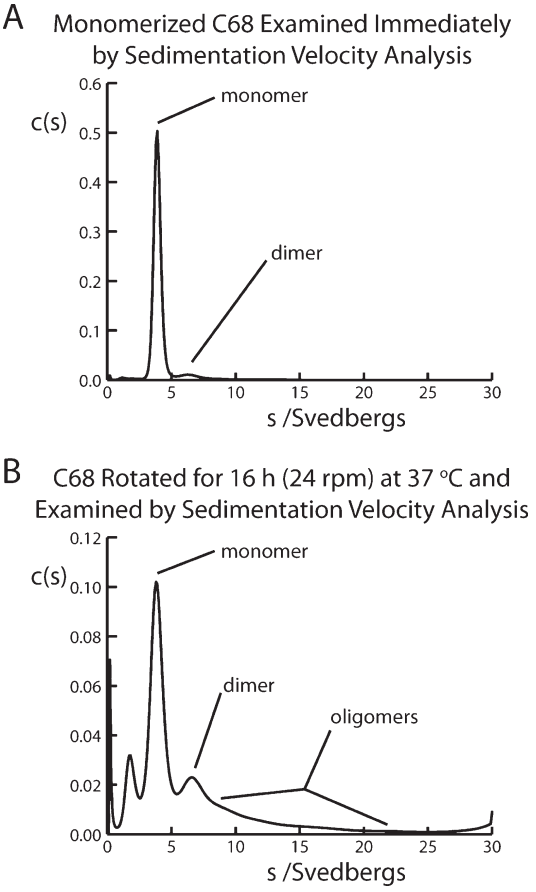

FIGURE 2: C68 was examined by analytical ultracentrifugation (AUC) to quantify the presence of monomer, dimer, trimer, or higher-order oligomeric species. Values for integration of the peaks are given in the text. (A) Freshly monomerized C68 (3 μM) exhibits one major peak corresponding to a monomer. (B) Monomerized C68 (3 μM) was subjected to overhead rotation (24 rpm) for 16 h before analysis by AUC velocity experiments to demonstrate the presence of higher-order species in addition to the monomer peak.

fibrils are formed at pH 6.5 (Figure 6D of the Supporting Information).

To analyze potential oligomerization by AUC, an initially monomeric solution of C68 (4 μM) that was rotated for 16 h (24 rpm) at 37 °C was compared to a freshly monomerized C68 solution (4 μM). Although there was no evidence of a rapidly sedimenting species that would be observed for amyloid fibrils or large oligomers, the sedimentation velocity experiment is fully supportive of reversible soluble oligomer formation. For freshly monomerized C68 (Figure 2A), a peak with a sedimentation coefficient of 4.0 S, representing 92% of the sample, corresponds to the molecular weight of the monomer. A small peak at 6.8 S, representing 6% of the sample, is consistent with the molecular weight of a C68 dimer. If the sample is rotated overnight, a much higher percentage is oligomeric (Figure 2B). The peak with a sedimentation coefficient of 3.8 S, consistent with the molecular weight of a monomer, represents only 45% of the sample. A substantial dimer peak at 6.8 S is present, along with shoulders, likely representing higher-order oligomers. Altogether, the oligomers represent 42% of the sample. The small peak with a sedimentation coefficient of 2.0 S is likely due to proteolysis.

Because no fibrils or high-molecular weight structures were observed by AFM, because the TfT fluorescence does not increase significantly, and because no rapidly sedimenting species were observed in the AUC experiments, we can conclude that the

68 kDa fragment does not form cross-β-sheet amyloid fibrils. Instead, it remains mostly monomeric, transiently populating dimers, trimers, and possibly tetramers.

The 8 and 5 kDa Gelsolin Fragments Aggregate by a Nucleated Polymerization Mechanism. A nucleated polymerization amyloidogenesis reaction is characterized by a lag phase, during which the amyloidogenic peptide forms a high-energy oligomer or nucleus, which is the rate-limiting step of fibril formation. Once the nucleus is formed, additional monomers can add to it in a fibril extension reaction, a thermodynamically favorable process characterized by a relatively rapid growth phase. The rapidity of the growth phase is also influenced by fibril fragmentation efficiency (*62*−*64*). Nucleation and fibril extension are concentration dependent (*62*, *65*) up to a certain protein concentration beyond which off-pathway aggregation may begin to occur, slowing the rate of fibril formation (*66*).

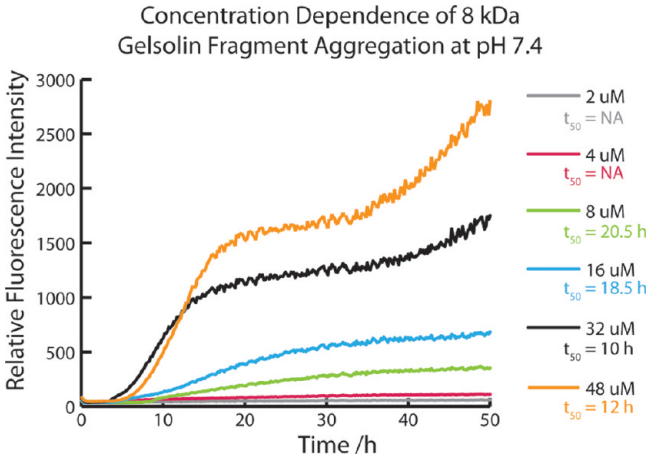

FIGURE 3: Concentration dependence of 8 kDa plasma gelsolin fragment amyloidogenesis analyzed at pH 7.4 using the TfT plate reader assay. Concentrations of the 8 kDa fragment ranged from 2 to 48 μM, as indicated. The t_{50} for each curve is defined as the time required to reach half the fluorescence at which the fibril extension reaction is completed and is shown in the legend.

As the concentration of the monomerized 8 kDa plasma gelsolin fragment increases from 2 to 32 μM, the lag phase becomes shorter and the rate of fibril extension increases (Figure 3). However, as the concentration of the monomerized 8 kDa fragment increases from 32 to 48 μM, the lag phase is slightly longer and the rate of amyloidogenesis begins to plateau, if not decrease, suggesting the onset of off-pathway aggregation. The lag phase associated with the aggregation of the 5 kDa peptide also becomes shorter as the concentration increases (Figure 7 of the Supporting Information). However, a minimum in the nucleation period or a maximum in the extension rate was not observed at the highest concentration employed (40 μM).

Another feature of a nucleated polymerization aggregation reaction is that the lag phase can be dramatically shortened or even eliminated via addition of preformed fibril seeds that bypass the requirement for nucleation (*67*). To determine whether gelsolin fragment amyloidogenesis exhibits this feature, increasing quantities of either 5 or 8 kDa gelsolin fragment preformed fibril seeds were added to the amyloid fibril formation assay. The addition of increasing quantities of 8 kDa seeds was shown to significantly decrease the nucleation period associated with 8 kDa gelsolin fragment amyloidogenesis (Figure 4A). The 5 kDa seeds were shown to similarly decrease the 8 kDa gelsolin fragment amyloidogenesis nucleation period (Figure 4B). In addition, 5 kDa gelsolin fragment fibril formation was accelerated and the nucleation period was proportionately decreased by

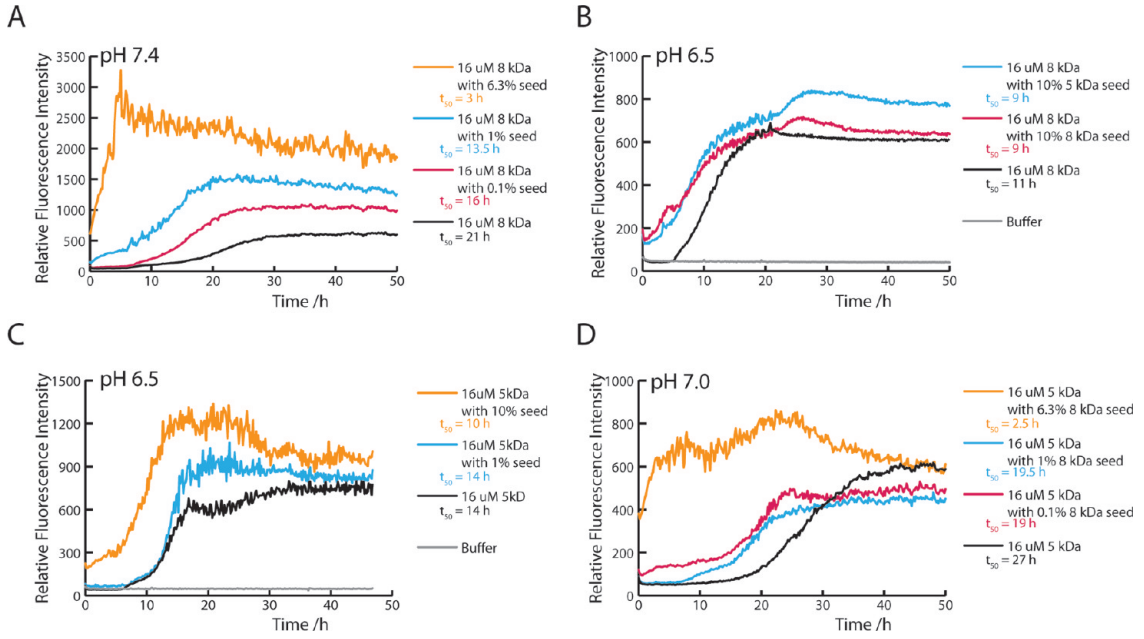

FIGURE 4: Addition of preformed amyloid fibrils or "seeds" accelerates 8 and 5 kDa gelsolin fragment amyloidogenesis. In each experiment, preformed fibrils were sonicated for 20 min to generate fibrils of uniform length, a known quantity of which were added to the solution at the start of the plate reader TfT fluorescence aggregation assay. The t_{50} for each curve is defined as the time required to reach half the fluorescence of the fibril extension reaction. The t_{50} values are shown in the legends. (A) Amyloidogenesis of the monomerized 8 kDa gelsolin fragment in the presence of increasing concentrations of preformed 8 kDa fibrils at pH 7.4. The final concentration of 8 kDa gelsolin fragment was 16 μM, including the added seed. (B) The addition of 10% 8 kDa seed was compared to the addition of 10% 5 kDa seed to the monomerized 8 kDa gelsolin fragment (14.4 μM, to give a final gelsolin fragment concentration of 16 μM). The pH for this experiment was 6.5. (C and D) Amyloidogenesis of the monomerized 5 kDa gelsolin fragment in the presence of various concentrations of preformed 5 kDa fibril seeds at pH 6.5 (C) and preformed 8 kDa fibril seeds at pH 7.0 (D). The final concentration of gelsolin fragment(s) was 16 μM, including the seed.

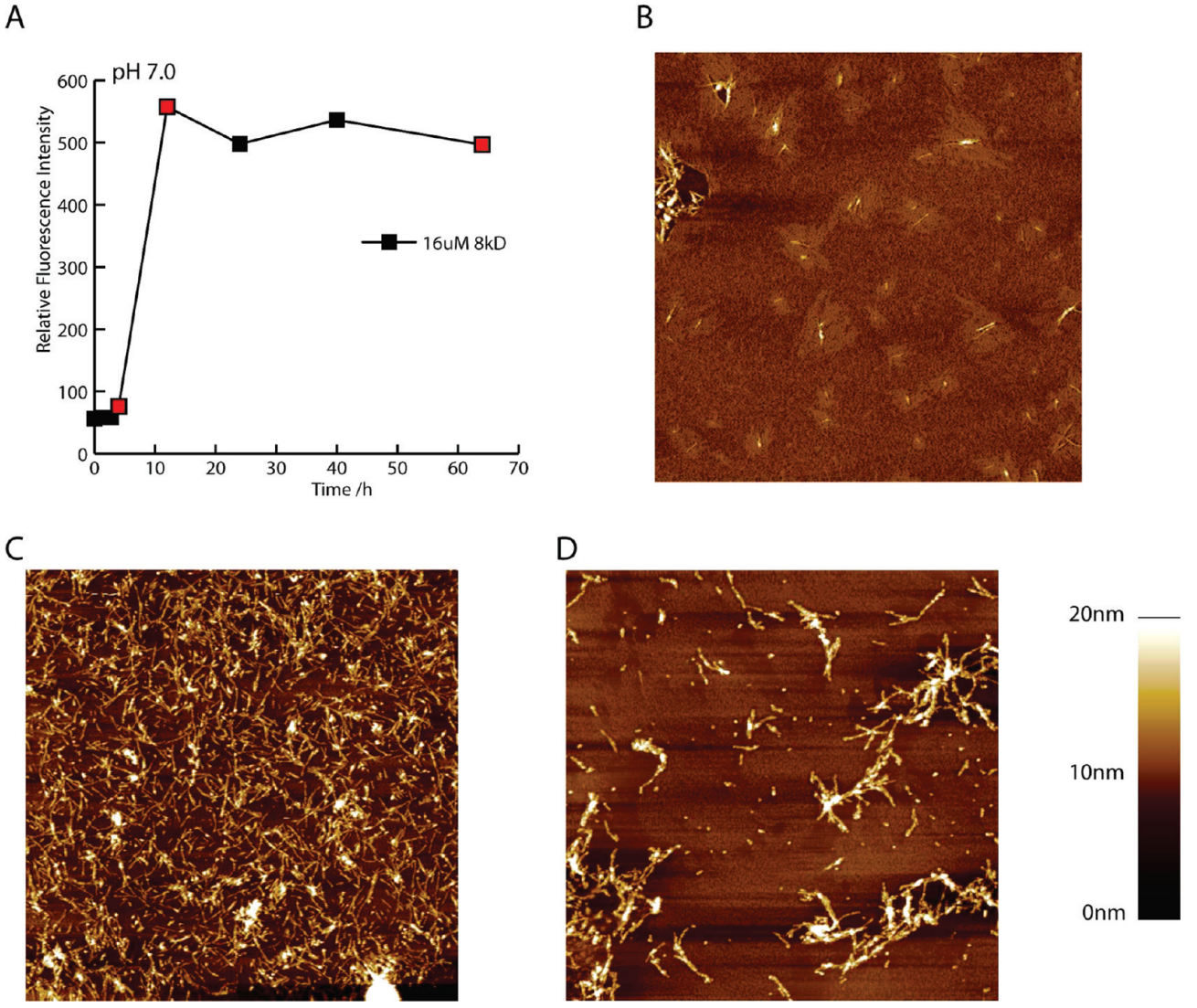

FIGURE 5: Freshly monomerized 8 kDa plasma gelsolin fragment solution (16 μM) mixed at pH 7.0 by overhead rotation (24 rpm) at 37 °C. (A) At various times indicated on the time course, an aliquot was removed and the TfT fluorescence was measured. At the three time points indicated by filled red squares (4, 12, and 64 h), the morphology of the fibrils was examined by atomic force microscopy (AFM). Each AFM image is a scan of a 5 μm × 5 μm area of the mica. (B) AFM image after the solution was mixed for 4 h (first red square), showing the presence of small fibrils and oligomers. (C) AFM image after the solution was mixed for 12 h (second red square) showing fully formed fibrils. (D) After continued mixing for 64 h (third red square), the AFM image shows laterally associated fibrils.

addition of either 5 and 8 kDa preformed fibrillar seeds (panels C and D of Figure 4, respectively).

The time dependence of the morphology of the aggregates formed by the 8 kDa gelsolin fragment (16 μM) was examined by AFM at three different time points in the nucleated polymerization aggregation reaction (Figure 5A). Figure 5B depicts the morphology of the aggregates formed at the beginning of the growth phase (4 h, first red data point). Figure 5C depicts the 8 kDa fibrillar aggregate morphology at the completion of the growth phase (12 h, second red data point). Figure 5D shows the laterally associated fibrils that are typically formed after a long stationary phase (64 h, third red data point). These time-dependent aggregate morphologies are precisely those expected from a nucleated polymerization fibrillization reaction. Unfortunately, the 5 kDa fibrils do not adhere to the mica and therefore could not be studied analogously by AFM.

Identification of the Cross-β-Sheet Core of the 8 and 5 kDa Gelsolin Amyloid Fibrils. The amino acid substructure of the 8 and 5 kDa gelsolin fragments comprising gelsolin's cross-β-sheet amyloid core is unknown. Since the portion of a peptide comprising the cross-β-sheet core of an amyloid fibril is resistant to proteolysis (*68*, *69*), the sequence comprising the gelsolin amyloid fibril core was probed by the established method of limited proteolytic digestion using proteinase K, a heat and chaotrope stable protease that is largely nonspecific but does exhibit some preference for cleaving after aliphatic and aromatic amino acids (*70*, *71*).

The proteinase K concentration and incubation period were first optimized via SDS−PAGE, and it was determined that an overnight incubation (16 h) of the fibrils using a proteinase K concentration of 3 μg/mL was optimal (Figure 8 of the Supporting Information). After digestion of the 8 kDa fibrils for 1 h, mass spectrometry revealed the presence of two peptides, one corresponding to a mass of 7860, which is the mass of the 8 kDa (amino acids 173−242) peptide itself, and one corresponding to a mass of 6831, which is the mass of the 60-mer sequence of amino acids 173−232. After overnight digestion, mass spectrometry revealed the presence of another peptide exhibiting a mass of 6595, corresponding to a 58-mer (amino acids 173−230), as the major product. The sequences of these peptides are listed in

Table 1: Proteinase K Resistant Core of the 8 and 5 kDa Plasma Gelsolin Amyloid Fibrils[a]

	amino acids	sequence	expected mass	actual mass
8 kDa fragment	173−242	ATEVPVSWESFNNGNCFILDLGNNIHQWCGSNSNRYERLKATQVSK-GIRDNERSGRARVHVSEEGTEPEA	7860.5	7860.1
8 kDa after 1 h	173−232	ATEVPVSWESFNNGNCFILDLGNNIHQWCGSNSNRYERLKATQVSK-GIRDNERSGRARVH	6831.5	6831.1
8 kDa after 16 h	173−230	ATEVPVSWESFNNGNCFILDLGNNIHQWCGSNSNRYERLKATQVSK-GIRDNERSGRAR	6595.2	6595.1
5 kDa fragment	173−225	ATEVPVSWESFNNGNCFILDLGNNIHQWCGSNSNRYERLKATQVSK-GIRDNER	6067.6	6067.6

[a]The proteinase K-treated 8 and 5 kDa fibrils (10 μL of a 0.15 mg/mL fibril solution) digested as a function of time were added to 90 μL of 8 M guanidine HCl and examined by LC−MS. The sequences of the fragments that resulted after proteinase K digestion are listed, along with their expected and actual masses.

Table 1. As a control, the freshly monomerized 8 kDa gelsolin fragment (40 μM) was subjected to the same concentration of proteinase K, and it was efficiently degraded by proteinase K, as no peaks were observed by ESI-MS (data not shown).

When the 5 kDa gelsolin fragment amyloid fibrils were digested overnight, no other band besides the 5 kDa fragment appeared in the SDS−PAGE gel, and mass spectrometry revealed only one species with a mass of 6067, corresponding to the 5 kDa (173−225) amyloidogenic fragment itself. Once again, the experimental masses of all these peptides were 2 units lower than the calculated theoretical masses of the reduced peptides due to the formation of a disulfide bond between the cysteines at positions 188 and 201. These data together suggest that the amyloid core is the 58-mer corresponding to amino acids 173−230.

DISCUSSION

A number of complementary approaches have been utilized to characterize the relative amyloidogenicities of the plasma gelsolin 68, 8, and 5 kDa fragments observed in FAF patients, as well as the mechanism by which the 8 and 5 kDa amyloidogenic fragments aggregate. While the C68 fragment exhibits a slight increase in TfT fluorescence with time, and the sedimentation velocity data convincingly demonstrated reversible oligomerization, no evidence of C68 amyloid fibril formation could be obtained, despite attempting a wide variety of experiments that often afford amyloid fibrils. In contrast, the 8 and 5 kDa FAF-associated gelsolin fragments were observed to aggregate into amyloid fibrils under a wide variety of conditions, by unseeded and seeded aggregation reactions, and by variable agitation methods. Concentration-dependent and seeding-accelerated aggregation reactions strongly suggest that the 8 and 5 kDa gelsolin FAF-associated fragments form amyloid fibrils by a nucleated polymerization mechanism. In this mechanism, the highest-energy species on the aggregation pathway is the nucleus, and after nucleation is achieved, fibril elongation occurs in a thermodynamically favorable fashion. Our kinetic observations regarding the 8 kDa gelsolin fragment amyloidogenesis reaction, when considered together with the visualization of oligomers by AFM at the beginning of the rapid growth phase of the polymerization, strongly support a nucleated polymerization mechanism.

When amyloid from FAF patients is isolated and characterized, more than 85% of the peptides composing the fibrils are found to be the 8 kDa fragment, with the remainder being the 5 kDa fragment (*42*). Notably, no C68 is observed in amyloid taken from FAF patients. These data are strictly consistent with the lack of C68 in amyloid extracted from a transgenic gelsolin amyloidosis mouse model (*19*). In the muscle of the D187N FAF mouse model, the 8 kDa fragment deposits as early as 6 weeks of age, whereas the 5 kDa fragment is not observed until ~12 months of age. All of these observations are consistent with our in vitro data, demonstrating that the 8 kDa fragment is more amyloidogenic than the 5 kDa fragment. Once the highly amyloidogenic 8 kDa fibril extension reaction begins in vivo, it could seed the fibrillization of the lower concentration of the 5 kDa monomer, as well as the 8 kDa monomer. This hypothesis, supported by the results outlined herein, offers an explanation for how amyloid load increases and likely explains why the 5 kDa peptide is not observed until later in the course of the disease; its in vivo concentration is lower, and it forms amyloid very slowly, if at all, until seeded by 8 kDa fibrils.

Integrating the data presented here with the biological data obtained from the FAF mouse model, we are able to draw some conclusions about the pathogenesis of gelsolin amyloidosis and to make some predictions. Full-length D187N/Y plasma gelsolin is cleaved within domain 2 in the trans Golgi network by furin, affording the C68 fragment. While it is possible that C68 forms oligomers, as evidenced by the AUC and the TfT data, these oligomers are not fibrillar in nature, and it is unlikely they form in vivo, because of the lack of an air−water interface.

It seems clear that the 8 and 5 kDa fragments are formed by the cleavage of C68 by active MT1-MMP (and possibly other proteases) on cells making C68, or on nearby cells, because in the mouse model, only the tissues that synthesize C68 cleave it into the amyloidogenic 8 and 5 kDa fragments, and only these tissues deposit 8 kDa gelsolin amyloid (*19*). It appears that high concentrations of sulfated oligosaccharides accelerate 8 kDa gelsolin aggregation, as the increasing population of glycosaminoglycans and 8 kDa amyloid correlates as the mice age (*19*, *24*). It is quite interesting that the core of the 8 kDa gelsolin fragment amyloid fibril is very similar to that of the 5 kDa fragment, yet the 8 kDa fragment aggregates faster, suggesting that the five extra amino acids in the β-sheet core (amino acids 226−230) or a subsequence not integral to the 8 kDa cross-β-sheet structure makes it aggregate faster.

The generation of the amyloidogenic 8 kDa plasma gelsolin fragment, and to a lesser extent the 5 kDa fragment, is clearly toxic to cells, apparently because of the process of amyloidogenesis, although the precise mechanism of proteotoxicity is anything but clear (*19*). The generation of these fragments and likely the subsequent process of amyloidogenesis ultimately lead to intracellular inclusion bodies made up of multiple proteins that contribute to muscle cell death, as observed in the FAF mouse model (*19*).

These biophysical studies, when considered in concert with the data from the FAF mouse model, support the hypothesis that the administration of an MT1-MMP inhibitor that is able to reach the muscle tissue should be effective at inhibiting the cleavage of C68 that forms the 8 and 5 kDa amyloidogenic fragments. Because it has been demonstrated that the C68 fragment is not amyloidogenic and does not appear to play a major part in FAF pathogenesis, it is likely that this treatment strategy would be effective at ameliorating FAF.

ACKNOWLEDGMENT

We thank Colleen Fearns and Lesley Page for helpful discussions and help with manuscript preparation, Huiqiao Susan Sun and Helen Lu Yin for the full-length plasma gelsolin construct and purification advice, and M. R. Ghadiri for use of his atomic force microscope.

SUPPORTING INFORMATION AVAILABLE

Representative trace from the final reverse phase HPLC purification of the 8 kDa gelsolin fragment resulting from CNBr cleavage (Figure 1), example LC−MS data from the purified 8 kDa gelsolin fragment (Figure 2), SDS−PAGE depiction of the purification methodology of C68 (Figure 3), SDS−PAGE depiction of the final purification step of full-length plasma gelsolin (Figure 4), relative amyloidogenicity of the 68, 8, and 5 kDa gelsolin fragments as measured by the increase in TfT fluorescence in the plate reader TfT aggregation assay at pH 7.0 and 7.4 (Figure 5), AFM analysis of a solution of C68 (4 μM) that was mixed by overhead rotation (24 rpm) at 37 °C overnight, where the AFM image is compared to that of a negative control of buffer alone and that of a positive control of a solution of 8 kDa fragment (4 μM) that was mixed by overhead rotation (24 rpm) at 37 °C overnight (Figure 6), concentration dependence of the 5 kDa plasma gelsolin fragment amyloidogenesis reaction analyzed at pH 6.5 using the TfT plate reader assay (concentrations of the 5 kDa fragment from 2 to 40 μM, as indicated) (Figure 7), and SDS−PAGE of proteinase K-digested 8 and 5 kDa fibrils (Figure 8). This material is available free of charge via the Internet at http://pubs.acs.org.

REFERENCES

1. Kelly, J. W. (1996) Alternative conformations of amyloidogenic proteins govern their behavior. *Curr. Opin. Struct. Biol. 6*, 11–17.
2. Kelly, J. W. (1998) The alternative conformations of amyloidogenic proteins and their multi-step assembly pathways. *Curr. Opin. Struct. Biol. 8*, 101–106.
3. Selkoe, D. J. (2003) Folding proteins in fatal ways. *Nature 426*, 900–904.
4. Dobson, C. M. (2003) Protein folding and misfolding. *Nature 426*, 884–890.
5. Cohen, F. E., and Kelly, J. W. (2003) Therapeutic approaches to protein-misfolding diseases. *Nature 426*, 905–909.
6. Sekijima, Y., Wiseman, R. L., Matteson, J., Hammarstrom, P., Miller, S. R., Sawkar, A. R., Balch, W. E., and Kelly, J. W. (2005) The biological and chemical basis for tissue-selective amyloid disease. *Cell 121*, 73–85.
7. Fandrich, M., Fletcher, M. A., and Dobson, C. M. (2001) Amyloid fibrils from muscle myoglobin: Even an ordinary globular protein can assume a rogue guise if conditions are right. *Nature 410*, 165–166.
8. Cohen, E., Bieschke, J., Perciavalle, R. M., Kelly, J. W., and Dillin, A. (2006) Opposing activities protect against age-onset proteotoxicity. *Science 313*, 1604–1610.
9. Gidalevitz, T., Ben-Zvi, A., Ho, K. H., Brignull, H. R., and Morimoto, R. I. (2006) Progressive disruption of cellular protein folding in models of polyglutamine diseases. *Science 311*, 1471–1474.
10. Morley, J. F., and Morimoto, R. I. (2004) Regulation of longevity in *Caenorhabditis elegans* by heat shock factor and molecular chaperones. *Mol. Biol. Cell 15*, 657–664.
11. Morley, J. F., Brignull, H. R., Weyers, J. J., and Morimoto, R. I. (2002) The threshold for polyglutamine-expansion protein aggregation and cellular toxicity is dynamic and influenced by aging in *Caenorhabditis elegans*. *Proc. Natl. Acad. Sci. U.S.A. 99*, 10417–10422.
12. Balch, W. E., Morimoto, R. I., Dillin, A., and Kelly, J. W. (2008) Adapting proteostasis for disease intervention. *Science 319*, 916–919.
13. Colon, W., and Kelly, J. W. (1992) Partial Denaturation of Transthyretin is Sufficient for Amyloid Fibril Formation in vitro. *Biochemistry 31*, 8654–8660.
14. Tanzi, R. E., and Bertram, L. (2005) Twenty years of the Alzheimer's disease amyloid hypothesis: A genetic perspective. *Cell 120*, 545–555.
15. Sanchorawala, V., Wright, D. G., Seldin, D. C., Dember, L. M., Finn, K., Falk, R. H., Berk, J., Quillen, K., and Skinner, M. (2001) An overview of the use of high-dose melphalan with autologous stem cell transplantation for the treatment of AL amyloidosis. *Bone Marrow Transplant. 28*, 637–642.
16. McCutchen, S. L., Lai, Z. H., Miroy, G. J., Kelly, J. W., and Colon, W. (1995) Comparison of Lethal and Nonlethal Transthyretin Variants and their Relationship to Amyloid Disease. *Biochemistry 34*, 13527–13536.
17. Kelly, J. W. (1998) The environmental dependency of protein folding best explains prion and amyloid diseases. *Proc. Natl. Acad. Sci. U.S.A. 95*, 930–932.
18. Westermark, P., Sletten, K., Johansson, B., and Cornwell, G. G. (1990) Fibril in Senile Systemic Amyloidosis Is Derived from Normal Transthyretin. *Proc. Natl. Acad. Sci. U.S.A. 87*, 2843–2845.
19. Page, L. J., Suk, J. Y., Bazhenova, L., Fleming, S. M., Wood, M., Jiang, Y., Guo, L. T., Mizisin, A. P., Kisilevsky, R., Shelton, G. D., Balch, W. E., and Kelly, J. W. (2009) Secretion of amyloidogenic gelsolin progressively compromises protein homeostasis leading to the intracellular aggregation of proteins. *Proc. Natl. Acad. Sci. U.S.A. 106*, 11125–11130.
20. Hiltunen, T., Kiuru, S., Hongell, V., Helio, T., Palo, J., and Peltonen, L. (1991) Finnish type of familial amyloidosis: Cosegregation of Asp187→Asn mutation of gelsolin with the disease in three large families. *Am. J. Hum. Genet. 49*, 522–528.
21. Maury, C. P., Kere, J., Tolvanen, R., and de la Chapelle, A. (1990) Finnish hereditary amyloidosis is caused by a single nucleotide substitution in the gelsolin gene. *FEBS Lett. 276*, 75–77.
22. Levy, E., Haltia, M., Fernandez-Madrid, I., Koivunen, O., Ghiso, J., Prelli, F., and Frangione, B. (1990) Mutation in gelsolin gene in Finnish hereditary amyloidosis. *J. Exp. Med. 172*, 1865–1867.
23. Sunada, Y., Shimizu, T., Mannen, T., and Kanazawa, I. (1992) [Familial amyloidotic polyneuropathy type IV (Finnish type): The first description of a large kindred in Japan]. *Rinsho Shinkeigaku 32*, 826–833.
24. Suk, J. Y., Zhang, F., Balch, W. E., Linhardt, R. J., and Kelly, J. W. (2006) Heparin Accelerates Gelsolin Amyloidogenesis. *Biochemistry 45*, 2234–2242.
25. Kiuru-Enari, S., Keski-Oja, J., and Haltia, M. (2005) Cutis laxa in hereditary gelsolin amyloidosis. *Br. J. Dermatol. 152*, 250–257.
26. Kiuru, S., Matikainen, E., Kupari, M., Haltia, M., and Palo, J. (1994) Autonomic Nervous System and Cardiac Involvement in Familial Amyloidosis, Finnish Type (FAF). *J. Neurol. Sci. 126*, 40–48.
27. Kivela, T., Tarkkanen, A., Frangione, B., Ghiso, J., and Haltia, M. (1994) Ocular amyloid deposition in familial amyloidosis, Finnish: An analysis of native and variant gelsolin in Meretoja's syndrome. *Invest. Ophthalmol. Visual Sci. 35*, 3759–3769.
28. Kiuru-Enari, S., Somer, H., Seppalainen, A. M., Notkola, I. L., and Haltia, M. (2002) Neuromuscular pathology in hereditary gelsolin amyloidosis. *J. Neuropathol. Exp. Neurol. 61*, 565–571.
29. Kiuru, S. (1998) Gelsolin-related familial amyloidosis, Finnish type (FAF), and its variants found worldwide. *Amyloid 5*, 55–66.
30. Burtnick, L. D., Koepf, E. K., Grimes, J., Jones, E. Y., Stuart, D. I., Mclaughlin, P. J., and Robinson, R. C. (1997) The crystal structure of plasma gelsolin: Implications for actin severing, capping, and nucleation. *Cell 90*, 661–670.
31. Sun, H. Q., Yamamoto, M., Mejillano, M., and Yin, H. L. (1999) Gelsolin, a multifunctional actin regulatory protein. *J. Biol. Chem. 274*, 33179–33182.
32. DiNubile, M. J. (2008) Plasma gelsolin as a biomarker of inflammation. *Arthritis Res. Ther. 10*, 2.
33. Lee, P. S., Sampath, K., Karumanchi, S. A., Tamez, H., Bhan, I., Isakova, T., Gutierrez, O. M., Wolf, M., Chang, Y., Stossel, T. P., and

Thadhani, R. (2009) Plasma gelsolin and circulating actin correlate with hemodialysis mortality. *J. Am. Soc. Nephrol. 20*, 1140–1148.
34. Kwiatkowski, D. J., Mehl, R., Izumo, S., Nadalginard, B., and Yin, H. L. (1988) Muscle is the Major Source of Plasma Gelsolin. *J. Biol. Chem. 263*, 8239–8243.
35. Chen, C. D., Huff, M. E., Matteson, J., Page, L. J., Phillips, R., Kelly, J. W., and Balch, W. E. (2001) Furin initiates gelsolin familial amyloidosis in the Golgi through a defect in Ca^{2+} stabilization. *EMBO J. 20*, 6277–6287.
36. Kazmirski, S. L., Isaacson, R. L., An, C., Buckle, A., Johnson, C. M., Daggett, V., and Fersht, A. R. (2002) Loss of a metal-binding site in gelsolin leads to familial amyloidosis-Finnish type. *Nat. Struct. Biol. 9*, 112–116.
37. Huff, M. E., Page, L. J., Balch, W. E., and Kelly, J. W. (2003) Gelsolin domain 2 Ca^{2+} affinity determines susceptibility to furin proteolysis and familial amyloidosis of Finnish type. *J. Mol. Biol. 334*, 119–127.
38. Kangas, H., Seidah, N. G., and Paunio, T. (2002) Role of Proprotein Convertases in the Pathogenic Processing of the Amyloidosis-associated Form of Secretory Gelsolin. *Amyloid 9*, 83–87.
39. Nag, S., Ma, Q., Wang, H., Chumnarnsilpa, S., Lee, W. L., Larsson, M., Kannan, B., Hernandez-Valladarez, M., Burtnick, L. D., and Robinson, R. C. (2009) Ca^{2+} binding by domain 2 plays a critical role in the activation and stabilization of gelsolin. *Proc. Natl. Acad. Sci. U.S.A. 106*, 13713–13718.
40. Witke, W., Sharpe, A. H., Hartwig, J. H., Azuma, T., Stossel, T. P., and Kwiatkowski, D. J. (1995) Hemostatic, Inflammatory, and Fibroblast Responses Are Blunted in Mice Lacking Gelsolin. *Cell 81*, 41–51.
41. Page, L. J., Suk, J. Y., Huff, M. E., Lim, H. J., Venable, J., Yates, J., Kelly, J. W., and Balch, W. E. (2005) Metalloendoprotease cleavage triggers gelsolin amyloidogenesis. *EMBO J. 24*, 4124–4132.
42. Maury, C. P. J. (1991) Gelsolin Related Amyloidosis: Identification of the Amyloid Protein in Finnish Hereditary Amyloidosis as a Fragment of Variant Gelsolin. *J. Clin. Invest. 87*, 1195–1199.
43. Robinson, R. C., Choe, S. Y., and Burtnick, L. D. (2001) The disintegration of a molecule: The role of gelsolin in FAF, familial amyloidosis (Finnish type). *Proc. Natl. Acad. Sci. U.S.A. 98*, 2117–2118.
44. Liepina, I., Janmey, P., Czaplewski, C., and Liwo, A. (2004) Towards gelsolin amyloid formation. *Biopolymers 76*, 543–548.
45. Ratnaswamy, G., Koepf, E., Bekele, H., Yin, H., and Kelly, J. W. (1999) The amyloidogenicity of gelsolin is controlled by proteolysis and pH. *Chem. Biol. 6*, 293–304.
46. Yonemoto, I. T., Wood, M. R., Balch, W. E., and Kelly, J. W. (2009) A general strategy for the bacterial expression of amyloidogenic peptides using BCL-XL-1/2 fusions. *Protein Sci. 18*, 1978–1986.
47. Yu, F. X., Zhou, D. M., and Yin, H. L. (1991) Chimeric and Truncated gCap39 Elucidate the Requirements for Actin Filament Severing and End Capping by the Gelsolin Family of Proteins. *J. Biol. Chem. 266*, 19269–19275.
48. Bieschke, J., Zhang, Q., Powers, E. T., Lerner, R. A., and Kelly, J. W. (2005) Oxidative metabolites accelerate Alzheimer's amyloidogenesis by a two-step mechanism, eliminating the requirement for nucleation. *Biochemistry 44*, 4977–4983.
49. Schuck, P. (2000) Size-distribution analysis of macromolecules by sedimentation velocity ultracentrifugation and lamm equation modeling. *Biophys. J. 78*, 1606–1619.
50. Schagger, H., and Von Jagow, G. (1987) Tricine Sodium Dodecyl-Sulfate Polyacrylamide-Gel Electrophoresis for the Separation of Proteins in the Range from 1 to 100 kDa. *Anal. Biochem. 166*, 368–379.
51. Pawar, A. P., DuBay, K. F., Zurdo, J., Chiti, F., Vendruscolo, M., and Dobson, C. M. (2005) Prediction of "aggregation-prone" and "aggregation-susceptible" regions in proteins associated with neurodegenerative diseases. *J. Mol. Biol. 350*, 379–392.
52. Hurshman, A. R., White, J. T., Powers, E. T., and Kelly, J. W. (2004) Transthyretin aggregation under partially denaturing conditions is a downhill polymerization. *Biochemistry 43*, 7365–7381.
53. Lindgren, M., Sorgjerd, K., and Hammarstrom, P. (2005) Detection and characterization of aggregates, prefibrillar amyloidogenic oligomers, and protofibrils using fluorescence spectroscopy. *Biophys. J. 88*, 4200–4212.
54. Groenning, M., Olsen, L., van de Weert, M., Flink, J. M., Frokjaer, S., and Jorgensen, F. S. (2007) Study on the binding of thioflavin T to β-sheet-rich and non-β-sheet cavities. *J. Struct. Biol. 158*, 358–369.
55. Alexandrescu, A. T. (2005) Amyloid accomplices and enforcers. *Protein Sci. 14*, 1–12.
56. Meng, F., Abedini, A., Song, B., and Raleigh, D. P. (2007) Amyloid formation by pro-islet amyloid polypeptide processing intermediates: Examination of the role of protein heparan sulfate interactions and implications for islet amyloid formation in type 2 diabetes. *Biochemistry 46*, 12091–12099.
57. Vernaglia, B. A., Huang, J., and Clark, E. D. (2004) Guanidine hydrochloride can induce amyloid fibril formation from hen egg-white lysozyme. *Biomacromolecules 5*, 1362–1370.
58. Sicorello, A., Torrassa, S., Soldi, G., Gianni, S., Travaglini-Allocatelli, C., Taddei, N., Relini, A., and Chiti, F. (2009) Agitation and High Ionic Strength Induce Amyloidogenesis of a Folded PDZ Domain in Native Conditions. *Biophys. J. 96*, 2289–2298.
59. Sluzky, V., Tamada, J. A., Klibanov, A. M., and Langer, R. (1991) Kinetics of Insulin Aggregation in Aqueous Solutions upon Agitation in the Presence of Hydrophobic Surfaces. *Proc. Natl. Acad. Sci. U.S.A. 88*, 9377–9381.
60. Nayak, A., Dutta, A. K., and Belfort, G. (2008) Surface-enhanced nucleation of insulin amyloid fibrillation. *Biochem. Biophys. Res. Commun. 369*, 303–307.
61. Sethuraman, A., Vedantham, G., Imoto, T., Przybycien, T., and Belfort, G. (2004) Protein unfolding at interfaces: Slow dynamics of α-helix to β-sheet transition. *Proteins: Struct., Funct., Bioinf. 56*, 669–678.
62. Ferrone, F. (1999) Analysis of protein aggregation kinetics. In Amyloid, Prions, and Other Protein Aggregates, pp 256−274, Academic Press, San Diego.
63. Collins, S. R., Douglass, A., Vale, R. D., and Weissman, J. S. (2004) Mechanism of prion propagation: Amyloid growth occurs by monomer addition. *PLoS Biol. 2*, 1582–1590.
64. Xue, W. F., Homans, S. W., and Radford, S. E. (2008) Systematic analysis of nucleation-dependent polymerization reveals new insights into the mechanism of amyloid self-assembly. *Proc. Natl. Acad. Sci. U.S.A. 105*, 8926–8931.
65. Powers, E. T., and Powers, D. L. (2006) The kinetics of nucleated polymerizations at high concentrations: Amyloid fibril formation near and above the "supercritical concentration". *Biophys. J. 91*, 122–132.
66. Powers, E. T., and Powers, D. L. (2008) Mechanisms of protein fibril formation: Nucleated polymerization with competing off-pathway aggregation. *Biophys. J. 94*, 379–391.
67. Hortschansky, P., Schroeckh, V., Christopeit, T., Zandomeneghi, G., and Fandrich, M. (2005) The aggregation kinetics of Alzheimer's β-amyloid peptide is controlled by stochastic nucleation. *Protein Sci. 14*, 1753–1759.
68. Frare, E., Mossuto, M. F., de Laureto, P. P., Dumoulin, M., Dobson, C. M., and Fontana, A. (2006) Identification of the core structure of lysozyme amyloid fibrils by proteolysis. *J. Mol. Biol. 361*, 551–561.
69. Myers, S. L., Thomson, N. H., Radford, S. E., and Ashcroft, A. E. (2006) Investigating the structural properties of amyloid-like fibrils formed in vitro from β2-microglobulin using limited proteolysis and electrospray ionisation mass spectrometry. *Rapid Commun. Mass Spectrom. 20*, 1628–1636.
70. Ebeling, W., Hennrich, N., Klockow, M., Metz, H., Orth, H. D., and Lang, H. (1974) Proteinase K from *Tritirachium album* Limber. *Eur. J. Biochem. 47*, 91–97.
71. Betzel, C., Pal, G. P., and Saenger, W. (1988) 3-Dimensional Structure of Proteinase-K at 0.15-nm Resolution. *Eur. J. Biochem. 178*, 155–171.